Physical mechanisms of amyloid nucleation on fluid membranes

Johannes Krausser,[1,2] Tuomas P. J. Knowles,[3,4] and Anđela Šarić[1,2,*]

[1] *Department of Physics and Astronomy, Institute for the Physics of Living Systems, University College London, London WC1E 6BT, UK*
[2] *MRC Laboratory for Molecular Cell Biology, University College London, London WC1E 6BT, UK*
[3] *Department of Chemistry, University of Cambridge, Lensfield Road, Cambridge CB2 1EW, UK.*
[4] *Cavendish Laboratory, University of Cambridge, Cambridge CB3 0HE, UK*

Biological membranes can dramatically accelerate the aggregation of normally soluble protein molecules into amyloid fibrils and alter the fibril morphologies, yet the molecular mechanisms through which this accelerated nucleation takes place are not yet understood. Here, we develop a coarse-grained model to systematically explore the effect that the structural properties of the lipid membrane and the nature of protein-membrane interactions have on the nucleation rates of amyloid fibrils. We identify two physically distinct nucleation pathways and quantify how the membrane fluidity and protein-membrane affinity control the relative importance of those molecular pathways. We find that the membrane's susceptibility to reshaping and being incorporated into the fibril nucleus is a key determinant of its ability to promote protein aggregation. We then characterise the rates and the free energy profile associated to this heterogeneous nucleation process in which the surface itself participates in the aggregate structure. Finally, we compare quantitatively our data to experiments on membrane-catalysed amyloid aggregation of α-synuclein, a protein implicated in Parkinson's disease that predominately nucleates on membranes. More generally, our results provide a framework for understanding macromolecular aggregation on lipid membranes in a broad biological and biotechnological context.

INTRODUCTION

The aggregation of normally soluble proteins into β-sheet rich amyloid fibrils is a common form of protein assembly that has broad implications across biomedical and biotechnological sciences, in context as diverse as the molecular origins of neurodegenerative disorders to the production of functional materials [1, 2]. The presence of surfaces and interfaces can strongly influence amyloid aggregation, either catalysing or inhibiting it, depending on the nature of the surface. This effect has previously been studied for the cases of amyloid nucleation on nanoparticles [3–5], flat surfaces [6, 7], and on the surface of amyloid fibrils themselves [8, 9].

Lipid bilayers are a unique type of surface, which is ubiquitous in biology and is the main contributor to the large surface-to-volume ratio characteristic of biological systems. They are highly dynamic self-assembled structures that can induce structural changes in the proteins bound to them [10, 11] and markedly affect protein aggregation propensities [12, 13]. Increasing experimental evidence supports the principle that the interaction between amyloidogenic proteins and the lipid cell membrane catalyses *in vivo* amyloid nucleation involved in debilitating pathologies. For instance, it has been shown that lipid membranes can enhance the kinetics of α-synuclein aggregation, the protein involved in Parkinson's disease, by over three orders of magnitude with respect to homogeneous nucleation in solution [14].

Bilayer membranes can exist in different structural phases and can undergo local and global phase changes. A large body of work has focussed on exploring how the membrane's dynamical properties, such as its fluidity, influence amyloid aggregation of bound proteins. For instance, fluid membranes, constituted of short and saturated lipid chains, were found to most effectively catalyse the nucleation of α-synuclein [15], while less fluid membranes composed of long saturated lipid chains had less catalytic power. Furthermore, the addition of cholesterol to lipid membranes was found to alter its fluidity and govern the nucleation rate of Aβ42 [16], a peptide implicated in Alzheimer's disease. In these cases the physical properties of the membrane are controlled through variations in its composition, and decoupling the role of the membrane's physical properties from its chemical specificity is extremely challenging [15, 17, 18]. Computer simulations can be of great help in this case, enabling us to systematically investigate the role of the physical and chemical properties of lipid membranes independently from one another, thus helping to identify key players behind membrane-driven amyloid nucleation.

In this work, we develop a coarse-grained Monte-Carlo model for studying the nucleation of amyloidogenic proteins on lipid membranes. We use it to identify the microscopic mechanisms which connect the membrane properties, the rate of amyloid nucleation, and the morphology of amyloid aggregates. We find that the membrane most efficiently catalyses amyloid nucleation by donating its lipids to the nucleating fibril, which depends *i*) on the lipid solubility and often correlates with membrane fluidity and *ii*) the affinity of proteins to the membrane. This interdependence controls both the morphology of the resulting fibrils, which can range from protein-rich to lipid-rich, and the rate of fibril formation. We then discuss how our results provide a mechanistic explanation for a number of recent experimental observations

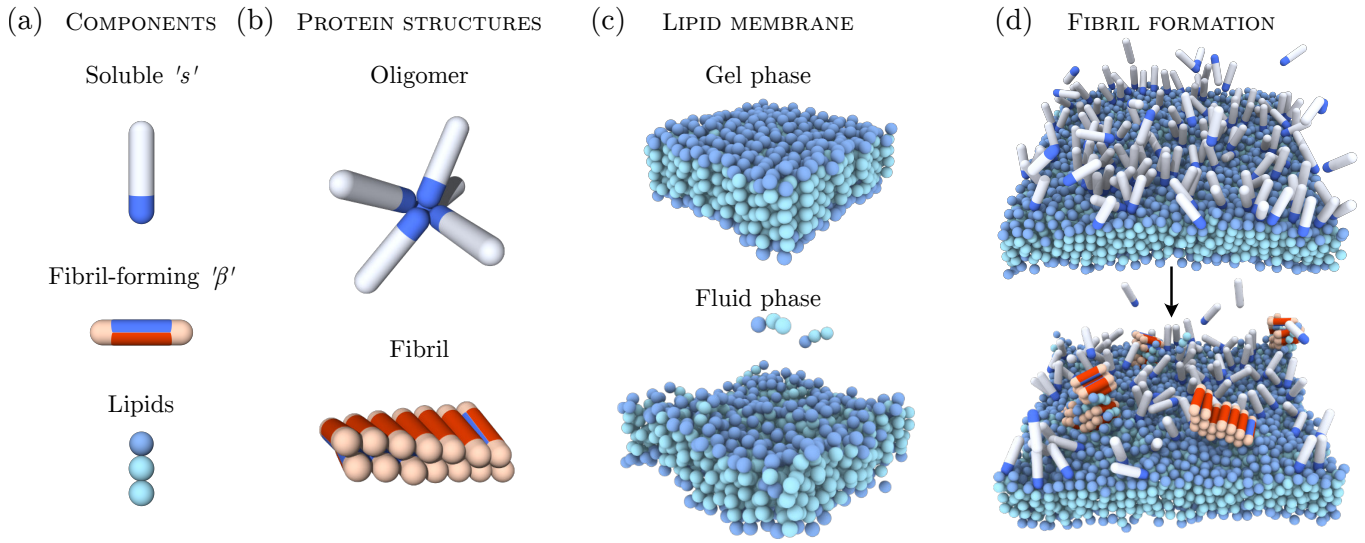

FIG. 1. **Simulation model and membrane-driven fibril formation. (a)** Proteins can exist in two distinct conformations: a soluble 's' and a β-sheet-prone conformation. Lipid molecules are modeled by one hydrophilic head and two hydrophobic tail beads. **(b)** Soluble proteins can form oligomers via their tip-to-tip interactions. Protein molecules in the β-sheet-forming conformation can assemble into fibrillar structures through the interactions of the blue side-patches. **(c)** The lipid membrane can exist in different structural phases depending on the inter-lipid interactions set in the model. Shown here are the gel phase ($k_{\mathrm{B}}T/\varepsilon = 0.775$) and fluid phase ($k_{\mathrm{B}}T/\varepsilon = 1.135$). **(d)** Example showing the formation of an amyloid fibril on the lipid membrane from bound proteins.

and offer a platform for studying strategies for bypassing amyloid nucleation in a cellular context.

RESULTS

Computational model

To study the essential features of membrane-assisted nucleation, we develop a coarse-grained computational model that takes into account the dynamic nature of the lipid membrane, the process of membrane-bound protein oligomerisation, and the protein structural transition that leads to fibril formation.

The lipid bilayer membrane is described using a previously published three-beads-per-lipid model [19], where the two hydrophobic tail beads are mutually attractive, allowing for the formation of a stable bilayer. We control the membrane's thermodynamic phase state by varying the depth of the interaction potential between the lipid tails, $k_{\mathrm{B}}T/\varepsilon$, where k_{B} is the Boltzmann constant and T is the temperature. In particular, to evaluate the protein nucleation kinetics across different membrane phases, we tune $k_{\mathrm{B}}T/\varepsilon$ between 0.775 (gel phase) and 1.135 (fluid phase), as shown in Fig. 1(c) (see Methods for details).

The minimal model for the amyloid-forming proteins is based on the coarse-grained model introduced in Refs. [20, 21]. Proteins are modelled as hard patchy spherocylinders and can exist in two distinct conformational states: a soluble (s) and a β-sheet forming (β) conformation, both of which are equipped with different arrangements of interaction patches. This model captures the aggregation behaviour through the colloidal nature of the building blocks, and the internal dynamics of the protein through the internal degree of freedom associated to the s-to-β-sheet conformational transition.

Soluble proteins interact through an attractive end cap on the spherocylinder, which allows for the formation of unstructured protein oligomers, Fig. 1(a). The β-prone conformation has an attractive side patch instead of a cap, which mediates attractive interactions both with the s and β conformations facilitating the alignment of proteins and the formation of elongated fibrils. The s-state represents the conformational ensemble of protein molecules in their soluble states, for instance a random coil for both the $A\beta$ peptide and α-synuclein. The β-state describes the a conformation of the polypeptide chain which possesses strong intermolecular interactions as found in the β-sheet-rich cores of amyloid fibrils. Crucially, the proteins can undergo a structural transition between the soluble and β-sheet-forming state. This stochastic transition is penalised with a free energy barrier $\Delta F_{\mathrm{s}\to\beta} = 10\,k_{\mathrm{B}}T$, reflecting the fact that amyloidogenic proteins lose conformational entropy when converting from native to the β-sheet-prone state and are rarely found in the β-sheet conformation on their own.

Analysis of the simulation trajectories shows that membrane binding is first achieved by the soluble protein conformation, whose affinity for the lipid membrane heads is set by the value of $\varepsilon_{\mathrm{sm}}$. To model the amphi-

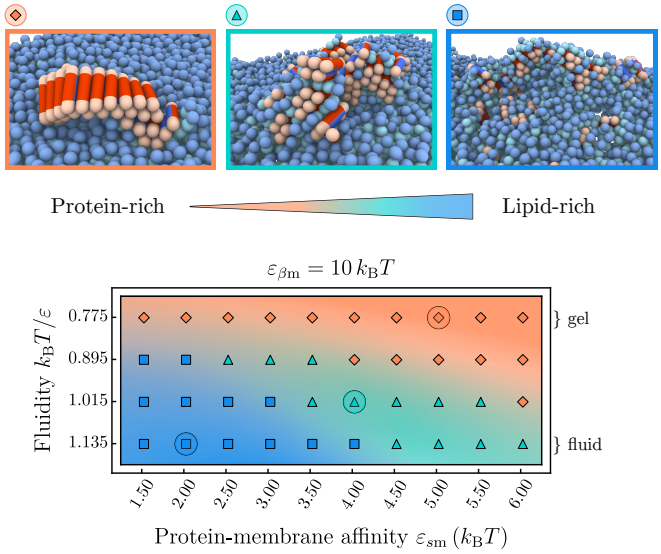

FIG. 2. **Morphologies of protein-lipid aggregates.** Phase space of the protein-lipid cluster morphologies depending on the membrane fluidity and protein-membrane affinity. Three main areas can be distinguished: extended fibrils (orange), smaller fibrillar clusters with interstitial lipids (green), and strongly mixed lipid-protein clusters (blue). The representative snapshots correspond to the circled parameter values; soluble proteins are not shown.

pathic nature of the protein and allow it to partially insert and anchor into the lipid membrane, as observed for both α-synuclein [22] and Aβ [23], the protein can also interact with the lipids tails with a fraction of ε_{sm}. The β-sheet-prone conformation is equipped with two separate patches on opposing sides of the spherocylinder with affinity for either the proteins or the lipids, Fig. 1(a). Such a twofold binding motif enables the protein to form a fibril and, at the same time, interact with the lipid membrane. This motif is chosen to mimic the general membrane-binding characteristics of amphipathic proteins such as α-synuclein and Aβ, which upon binding to the membrane can undergo a structural transition that promotes β-sheet formation in contact with lipids [10, 24, 25]. The strength of the lipophilic attraction of the protein (red patch) is controlled by $\varepsilon_{\beta m}$, while the protein-protein interaction with the s- and β-state (blue patch) are controlled by $\varepsilon_{s\beta}$ and $\varepsilon_{\beta\beta}$, respectively.

Membrane-assisted nucleation mechanisms

After subsequently binding to the bilayer, the soluble protein molecules can arrange into small oligomers on the membrane due to their self-interaction. Once a successful conversion in one of the proteins to its β-prone conformation has occurred, fibril aggregation can start. Our simulations show that the properties of lipid membranes can dramatically influence the pathway through which this nucleation occurs. In the following, we distinguish two basic pathways and the related morphologies of amyloid nuclei: a protein-rich and a lipid-rich, which also give rise to an intermediate case, as illustrated in the phase diagram in Fig. 2.

In the gel phase ($k_BT/\varepsilon = 0.775$), membrane lipids are packed closely and bound proteins are unlikely to penetrate into the bilayer. In this case, the membrane essentially behaves as a static surface: proteins adsorb onto the surface, form transient oligomers, which eventually provide an environment for fibril nucleation [20]. Such a pathway typically results in the appearance of elongated fibrils epitaxially growing on top of the bilayer (orange area in Fig. 2), which often detach and diffuse away from the membrane. The size of the fibrils strongly depends on the protein-membrane affinity ε_{sm}. High ε_{sm}-values lead to an increased membrane coverage, which causes fast growth of the fibril after initial conversion, and hence a higher proportion of longer fibrils, as shown in Supplementary Fig. A5.

The nucleation behaviour changes distinctly when the membrane is in the fluid phase, as best seen in the regime of low protein-lipid affinities in Fig. 2. In this case lipids are comparatively weakly bound within the bilayer and can easily be extracted from it. This enables the lipids to actively participate in the formation of fibril nuclei. At low protein-lipid affinities ε_{sm} the membrane is weakly covered by proteins and the first nucleation step typically proceeds via the direct interaction of a single protein with the hydrophobic tail of a lipid that has been extracted from the bilayer. The converted β-prone protein can then get coated in lipids or (partially) inserted into the lipid bilayer, which hampers the fast elongation of fibrils and leads to mixed protein-lipid clusters (blue area in Fig. 2). This nucleation pathway is promoted by packing defects in the lipid bilayer at increased membrane fluidities. The exact composition of the aggregates depends on the relative rate of incorporation of lipids and proteins into a nucleus, governed both by the membrane fluidity and the protein-membrane affinities.

At higher protein-membrane affinities ($\varepsilon_{sm} \gtrapprox 4\,k_BT$) the membrane is substantially covered by proteins, see Supplementary Fig. A2. The local environment of the nucleus will hence be abundant in soluble proteins, leading to a faster addition of protein monomers to fibril nuclei and hence fibrils with lower lipid content (green area in Fig. 3). Interestingly, the bound proteins also modify the local phase state of the membrane, as indicated by a reduction of the average area per lipid as ε_{sm} is increased (Supplementary Fig. A4). This hinders lipid extraction and yields an intermediate nucleation pathway between the lipid-rich and protein-rich regimes, as illustrated in Fig. 2.

Similar trends to those observed in our simulations have been reported in atomic force microscopy experiments monitoring Aβ aggregating on model lipid mem-

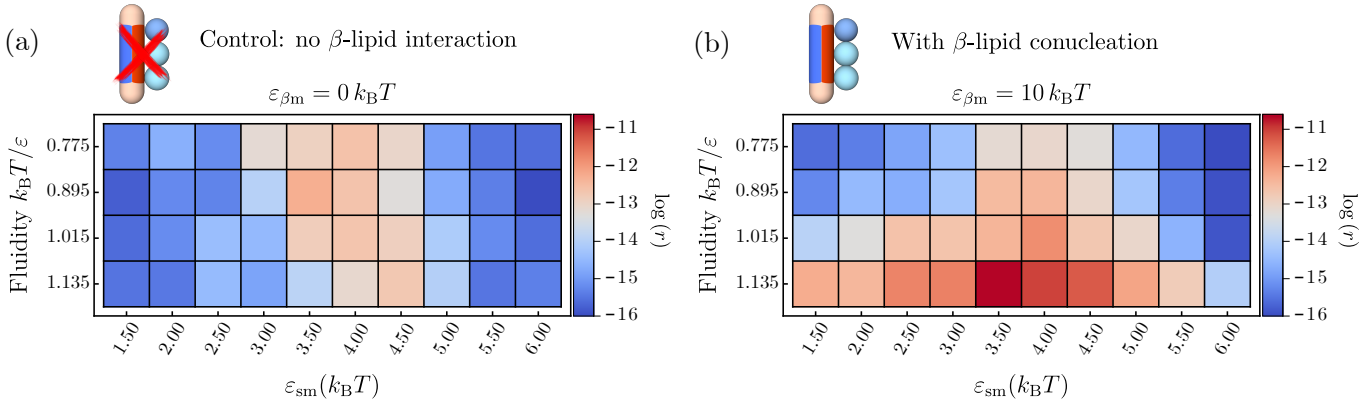

FIG. 3. **Amyloid nucleation rates on the membrane.** **(a)** Control case: nucleation rates when only soluble proteins interact with the lipid beads and β-like proteins do not penetrate into the hydrophobic core. Non-monotonic behaviour is observed with respect to the protein-lipid interaction ε_{sm}. **(b)** Nucleation rates when the interactions between the proteins and the lipid-tails are non-zero and proteins can penetrate the bilayer, as in Fig. 2. Amyloid nucleation is sped up in the direction of higher fluidities in addition to the non-monotonic scaling with ε_{sm} observed in (a).

branes [26]. On fluid model membranes with strong electrostatic interactions between proteins and lipids, bilayer deformations and clustering of lipids around Aβ were observed, whereas on gel phase membranes elongated mature fibrils appeared, just like in our simulations. Furthermore, experiments have shown that α-synuclein fibril formation in the presence of vesicles leads to membrane remodelling and lipid extraction [27], yielding fibrils intercalated with lipids that often cause vesicle disintegration. According behaviour involving membrane rupture can be observed in our simulations at later stages of the aggregation process when stresses induced by the growing fibril-lipid aggregates become too large.

Membrane fluidity enhances nucleation rates

In addition to controlling the morphologies of amyloid aggregates, the membrane has an immediate effect on the rates of amyloid nucleation. To convert from the soluble into the fibril-forming β-sheet-prone state the protein needs to overcome the intrinsic free energy barrier $\Delta F_{s\to\beta}$. The role of the membrane in modifying this nucleation barrier can be twofold: (i) to increase the local concentration of proteins by restricting their mobility to the membrane surface and (ii) to actively participate in the formation of the pre-fibrillar nucleus through hydrophobic interactions. Here, we decouple these two effects by analysing two separate scenarios: a control case in which a protein is only allowed to adsorb onto the membrane but cannot co-nucleate with lipids, and another one in which β-sheet-prone proteins can co-nucleate with lipids as in Fig. 3. The two scenarios are characterised by the presence or absence of the lipid-protein interaction patch of the β-prone conformation (red patch), while the interaction between the s-conformation and the lipids remains unaltered.

Starting with the control case, we remove the red patch by setting $\varepsilon_{\beta m} = 0\, k_B T$. As evident from Fig. 3(a), the nucleation rate $r(\varepsilon_{sm})$ is a non-monotonic function of the protein-membrane affinity ε_{sm}. Here, the rate $r(\varepsilon_{sm})$ is the inverse mean lag time of β-prone protein dimer formation. At small ε_{sm}-values the nucleation rates are low across all fluidities, where virtually no proteins are adsorbed onto the membrane. At intermediate membrane-protein affinities, the formation of stabilised membrane-bound oligomers lowers the nucleation barrier and increases the nucleation rates. At high membrane-protein affinities the nucleation process is inhibited due to the unfavourable free energy associated with nucleus detachment. Indeed at $\varepsilon_{\beta m} = 0\, k_B T$ the protein in the β-state loses its interaction with the membrane, which becomes costly at high protein-membrane affinities, hence prohibiting nucleation. The onset of this regime is systematically shifted to higher ε_{sm}-vales as the fluidity is increased. This is rooted in the fact that a higher lipid mobility inhibits the formation of stable oligomers on the membrane surface (Supplementary Fig. A3).

In the second scenario, the β-sheet-prone protein conformation carries a side patch with an affinity for the hydrophobic lipid tails of $\varepsilon_{\beta m} = 10\, k_B T$, rendering the protein amphipathic. Strikingly, the presence of the β-lipid interaction leads to a drastic change in the nucleation rates at higher membrane fluidities across all parameters pairs investigated, as shown in Fig. 3(b). This effect is caused by the progressive exposure of the membrane's hydrophobic core and the concomitant hydrophobic contacts between lipids and proteins. Loose lipid packing and the enhanced mobility of the lipids both in and out of the membrane plane enables the participation of lipids

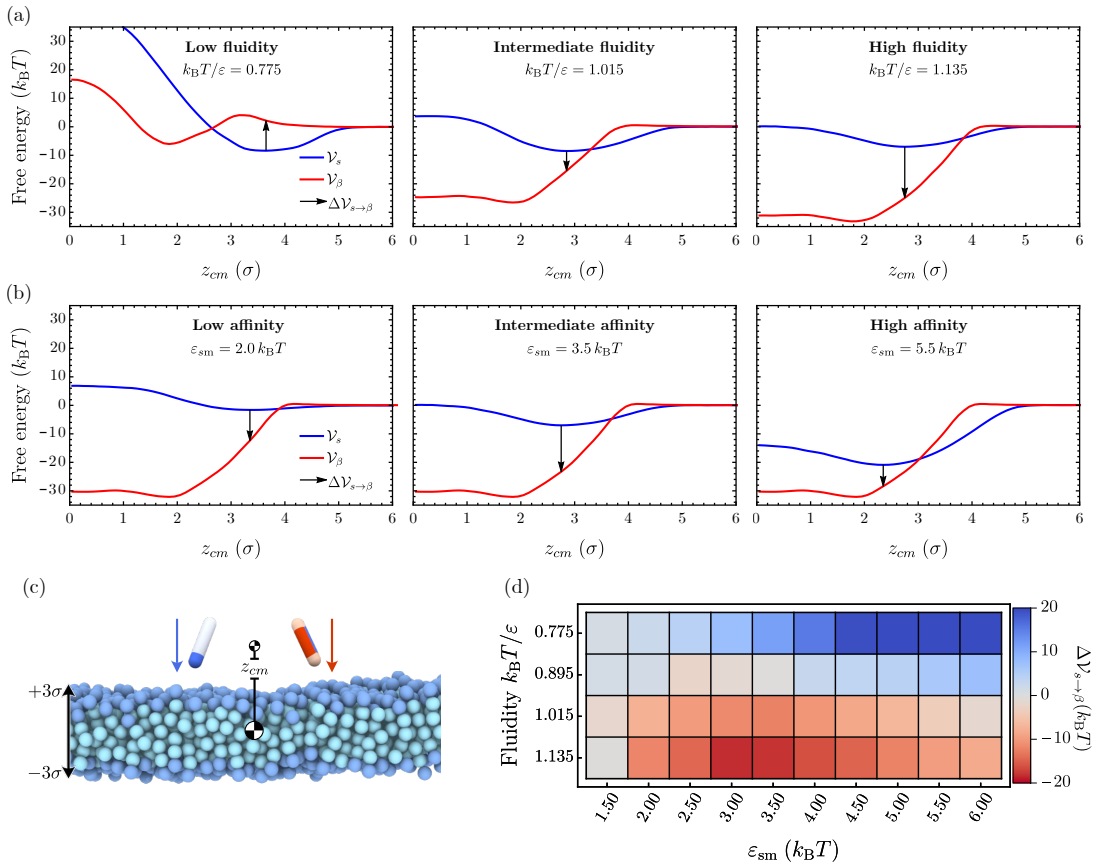

FIG. 4. **Changes in the potential of mean force at increasing membrane fluidity: (a), (b)** The three panels each show the free energy profiles $\mathcal{V}_s(z_{cm})$ (red) and $\mathcal{V}_\beta(z_{cm})$ (blue) at increasing fluidities $k_BT/\varepsilon = 0.775, 1.015$, and 1.135 while protein-membrane interactions are kept fixed at $\varepsilon_{sm} = 3.5\,k_BT$ and $\varepsilon_{\beta m} = 12\,k_BT$ **(a)**, and at increasing protein-membrane affinities $\varepsilon_{sm} = 2.0, 3.5$, and $5.5\,k_BT$ while the fluidity is kept fixed at $k_BT/\varepsilon = 1.135$ and $\varepsilon_{\beta m} = 12\,k_BT$ **(b)**. The arrows indicate the free energy cost for conformational conversion $\Delta\mathcal{V}$, providing a proxy for the nucleation barrier. **(c)** Initial snapshot of umbrella simulations for both particle species. **(d)** Difference between potentials of mean force in the 's' and 'β' conformation evaluated at the minimum of $\mathcal{V}_s(z)$ as a function of the membrane fluidity and the membrane-protein affinity ε_{sm}.

in the s-β conformational change and the formation of fibril nuclei.

The inclusion of lipids in protein aggregates efficiently drives fibril nucleation as the interaction between the lipid tails and proteins in the β-sheet prone conformation is favourable, which reduces the free energy barrier of the $s \to \beta$ conversion and stabilises fibril nuclei. This effect is more pronounced at increasing membrane fluidities that allow for better access to the hydrophobic regions of the lipid bilayer (Fig. 3). At the same time, a sufficiently but not too strong protein-membrane binding affinity ε_{sm} enables both efficient binding and cluster formation on the membrane without prohibiting the conformational conversion.

Free energy barrier for nucleation

To further characterise the molecular mechanisms of membrane-driven catalysis of amyloid aggregation, we investigate the free energy barriers connected to the different nucleation pathways. To this effect we sample the free energy landscape for the $s \to \beta$ conformational conversion of a protein along the protein-membrane centre-of-mass separation z_{cm} in different membrane environments, setting aside the effect of surface oligomerisation of the soluble proteins. First, we evaluate the free energy profile associated to a protein in either the s or β conformation interacting with the membrane, while separately varying the membrane fluidity and protein-membrane affinity, see Fig. 4.

Our simulations show that the free energy of binding between the membrane and the protein decreases with increasing fluidity, as evidenced by the results in Fig. 4(a) for $\varepsilon_{sm} = 3.5\,k_BT$ and $\varepsilon_{\beta m} = 12.0\,k_BT$ (see also Supplementary Fig. A8). Concurrently, we observe a softening of the repulsive contribution to the free energy profile $\mathcal{V}_s$ and a shift of its minimum to smaller z_{cm}-values. This change is the combined result of membrane thinning and a deeper average insertion of the protein into the bilayer

at high fluidities. Larger values of the membrane-protein affinity ε_{sm} at fixed fluidity entail both a deeper free energy minimum and a shift of the minimum position deeper into the hydrophobic core (Fig. 4 and Supplementary Fig. A8) . In the case of the protein in the β-conformation, the free energy profile $\mathcal{V}_\beta$ in the gel phase consists of a minimum located inside of the bilayer separated from the membrane surface by a small repulsive barrier, since it is energetically unfavourable for the β-protein to insert into the membrane at tight lipid packing (left panel in Fig. 4(a)). Increasing fluidity removes this barrier and $\mathcal{V}_\beta$ consists of one deep well representing the strong hydrophobic binding of the protein within the lipid membrane.

To estimate the free energy barrier for conversion between the protein's s- and β-conformation we evalaute the free energy difference $\Delta\mathcal{V} = \mathcal{V}_\beta - \mathcal{V}_\mathrm{s}$ at the equilibrium position of the soluble protein (indicated as a black arrow in Fig. 4). This free energy jump provides a proxy for the nucleation barrier in the dynamic Monte-Carlo simulations where soluble proteins first bind to the lipid and find their equilibrium position before slowly converting into the β-sheet-prone conformation. As evident from Fig. 4(a), as the membrane fluidity increases, the nucleation barrier $\Delta\mathcal{V}$ gradually disappears. Deeper insertion of the soluble protein permits strong interactions between the β-protein and the hydrophobic core of the membrane upon conformational conversion. Correspondingly, $\Delta\mathcal{V}$ becomes large and negative at high membrane fluidities, resulting in the increase in the nucleation rates (Fig. 4(d)).

Changing the affinity ε_{sm} can additionally influence the barrier. In the gel phase protein insertion into the membrane is not possible and we observe a monotonic increase of $\Delta\mathcal{V}(z)$ with higher protein-membrane affinities (top row of Fig. 4(d)). In the rate measurements reported in Fig. 3, the nucleation rate initially increased with ε_{sm} (lower $\Delta\mathcal{V}$) by virtue of surface oligomerisation. This is a multi-protein effect not captured at a level of a single protein conversion. Conversely, $\Delta\mathcal{V}$ becomes non-monotonic in ε_{sm} even without the multi-protein effects at high fluidities, since soluble proteins can partially insert into the fluid membrane. The interaction between the β-protein and lipid tails increases closer to the membrane centre, hence the free energy gain of transitioning to the β conformation also grows. In the strong binding regime, however, the effective binding free energy of the soluble protein grows faster than that of the β-prone protein, leading to the re-entrant increase in the free energy barrier $\Delta\mathcal{V}$ for the conformational conversion.

Quantitative comparison with experimental data

We compare our findings to experimental results [15], where the effect of lipid chemistry on the primary nucleation rates of α-synuclein has been investigated in the presence of lipid membranes. Considering fully saturated lipids of different acyl chain lengths, vesicles consisting of the longest acyl chains form gel-like membranes, which result in the slowest amyloid aggregation rates. Conversely, the shortest lipid molecules, which have the highest solubility in water and constitute a vesicle in the most fluid phase, lead to the fastest aggregation rates. Since our model is highly coarse-grained and general in nature, it remains non-trivial to map the exact lipid bilayer phase state and protein-membrane interaction parameters from experiments to our model. Nevertheless, the increase in the area per lipid between the gel and most fluid phase is between 30 and 40% in experiments, which closely matches the range we observe in simulations (Fig. 5). This is a parameter-free measurement that we can use to compare the simulation and experimental results. In experiments, the relative speed-up in the nucleation rate on fluid with respect to the gel-phase vesicle, $r_\mathrm{fluid}/r_\mathrm{gel}$, is a factor of approximately 5 for DMPS vesicles of medium fluidities and 20 for the most fluid DLPS vesicles, as illustrated in Fig. 5. This finding indeed compares very favourably with the results of our computational model, which predicts a closely matching range of the relative speed-up $r_\mathrm{fluid}/r_\mathrm{gel}$ at a given relative area per lipid $A_\mathrm{fluid}/A_\mathrm{gel}$, as shown in Fig. 5.

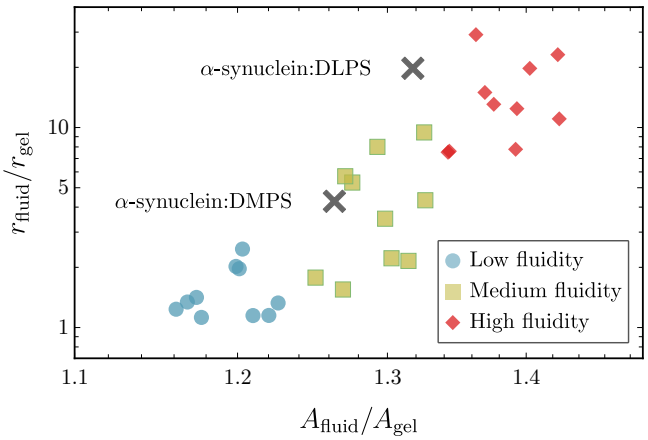

FIG. 5. **Comparison of simulation results with experimental data:** Comparison of the relative increase in nucleation rates $r_\mathrm{fluid}/r_\mathrm{gel}$ between the gel phase and fluid membranes as a function of the relative increase in area per lipid $A_\mathrm{fluid}/A_\mathrm{gel}$. Coloured symbols show simulation results at different fluidities: (blue) low fluidity ($k_\mathrm{B}T/\varepsilon = 0.895$), (green) medium fluidity ($k_\mathrm{B}T/\varepsilon = 1.015$) , and (red) high fluidity ($k_\mathrm{B}T/\varepsilon = 1.135$) with each subset containing 10 different ε_{sm}-values. The two black symbols represent experimental data from Ref. [15]. The experimental values for r_fluid and A_fluid of the fluid-phase DMPS and DLPS vesicles are normalised to r_gel and A_gel of a gel-phase DPPS vesicle, respectively.

DISCUSSION

In this work we present a coarse-grained simulation model to investigate how the phase state of a lipid membrane and membrane-protein binding affinity control the nucleation rates of amyloid fibrils. Depending on the specific amphipathic interaction motif of the amyloidogenic proteins, we identified two main nucleation mechanisms:

1. The formation of protein oligomers on the membrane surface and subsequent nucleation into pure fibrils

2. The mixing of membrane lipids with fibril-forming proteins enhanced by membrane fluidity.

The first mechanism determines the aggregation process when the protein cannot interact with the membrane hydrophobic core. The efficiency of this mechanism is dictated predominantly by the protein-membrane affinity, which stabilises oligomers on the membrane surface. The enhancement of nucleation is limited to a narrow regime of protein-membrane interaction in this case. Interestingly, this effect can be inhibited at high lipid mobilities, where the formation of stable oligomers becomes prohibited. This nicely illustrates that the membrane fluidity *per se* does not catalyse nucleation, but that specific interactions between the protein and the lipids, which often correlate with lipid fluidity, are required.

In fact, when interactions of the protein with the hydrophobic membrane core are present, a second more powerful nucleation mechanism is enabled. In this regime lipids can co-nucleate with proteins, which effectively lowers the nucleation barrier for their conformational conversion and can result in the formation of lipoprotein clusters. This mechanism depends crucially on the membrane fluidity and is enhanced by the presence of packing defects and lipid extraction from the bilayer. Indeed, considering the scenario where the protein in the β-sheet-prone state interacts with the lipid tails, we observe a 250-fold speed-up of the nucleation rates between the slowest and fastest cases in the gel and fluid phase, respectively, (Fig. 3b). This is contrasted by only a 20-fold speed-up for the case when the protein cannot interact with the lipid tails ($\varepsilon_{\beta\mathrm{m}} = 0\, k_{\mathrm{B}}T$) shown in Fig. 3(a).

Notably, we demonstrate that the window of effective nucleation is significantly broadened by the interaction between the protein and the membrane core leading to even more efficient amyloid nucleation over a wider range of membrane fluidities and protein affinities.

It is important to note that the membrane fluidity in our model is controlled only by inter-lipid interactions, hence the fluidity and the ability of lipids to be extracted from the bilayer are necessarily correlated in our model. This is a good representation for saturated lipids, where lipid solubility controls the phase state of the membrane. However, membrane phase behaviour can also be controlled by lipid geometry, as in the case of polyunsaturated lipids. In such a system the membrane fluidity and lipid solubility are not necessarily correlated in a straightforward way [14]. Similarly, membrane inclusions such as cholesterol [16] or proteins can also control the membrane phase behaviour and have a non-trivial effect on the ability to extract lipids from the bilayer. Our simulations do not capture these more complex couplings.

We found that the nature of the interactions between the protein and the membrane is of key importance in determining the aggregation pathway and the protein's capacity to disrupt membranes. In our model, the choice of two separate side patches is necessary to capture the incorporation of lipids into amyloid structures observed in experiments. Without a separate protein-lipid patch lipids are pushed out of fibrils and mixed aggregates cannot be achieved ruling out the pathway to lipid-rich aggregates.

Hence, the imbalance between membrane-membrane and membrane-protein interactions is an important factor not only in controlling the rates and pathways of amyloid aggregation, but also in determining whether amyloid aggregates are highly cytotoxic or not. This is also highlighted in a recent experimental study which shows that α-synuclein oligomers require a β-sheet core to insert themselves into the membrane bilayer and drive disruption of the bilayer [28].

The physical principles identified in this work are general in nature and applicable to a wide range of amyloid-forming proteins, irrespective of their sequence or fold. Even more, the presented mechanisms can also be of relevance to membrane-driven aggregation of other proteins that involve conformational changes and hydrophobic interactions. The computer model developed here also opens the way for testing strategies to bypass membrane-assisted amyloid aggregation, which can for instance involve targeting the interaction between proteins and membrane hydrophobic core, or altering the lipid composition to prevent protein-lipid co-nucleation.

ACKNOWLEDGMENTS

We are grateful to T. C. T. Michaels for reading the manuscript. We acknowledge support from the Academy of Medical Science (JK and AS), the Cambridge Centre for Misfolding Diseases (TPJK), the BBSRC (TPJK), the Frances and Augustus Newman foundation (TPJK), the ERC grant PhysProt (agreement n° 337969), Wellcome Trust (AS and TPJK), the Royal Society (AS), and the UK Materials and Molecular Modelling Hub for computational resources, which is partially funded by EPSRC (EP/P020194/1).

METHODS

Simulation model The coarse-grained simulation model employed in this study merges a minimal model of amyloid nucleation in solution [20] with a lipid bilayer implicit solvent model [19]. Proteins are represented by hard spherocylinders of diameter σ and length $\ell = 4\sigma$ and can exists in a soluble and a β-sheet forming conformation, as discussed in the main text. The membrane lipids are represented by a one head bead and two tail beads. Both the dynamics of the membrane-protein system and the conformational switches of the proteins are simulated using a Metropolis Monte-Carlo algorithm.

As depicted in Fig. 1(a), the soluble protein has an attractive end cap which allows it to form oligomeric structures. The pair-wise interaction between two soluble protein tips at distance $r = |\boldsymbol{r}|$ is given by

$$V_{ss} = \begin{cases} -\varepsilon_{ss}\left(\dfrac{\sigma}{r}\right)^6 & r \leq 1.3\,\sigma \\ 0 & r > 1.3\,\sigma. \end{cases} \tag{1}$$

with $\varepsilon_{ss} = 4\,k_{\mathrm{B}}T$ in this study. In the β-sheet forming conformation the spherocylinder has two attractive side patches instead of a tip interaction. One patch with affinity for the membrane, the other with affinity for other proteins.

The attractive protein side patch has the length of 0.7ℓ and an opening angle of 180°. If the two patches are facing each other mediates the interaction potential

$$V_{\beta\beta} = \begin{cases} -\varepsilon_{\beta\beta}\cos^2(\phi) - \varepsilon_{\beta\beta}\dfrac{\sigma}{r} & d \leq 1.3\,\sigma \\ 0 & d > 1.3\,\sigma \end{cases} \tag{2}$$

where d is the minimal distance between the interacting hydrophobic patches and $\varepsilon_{\beta\beta} = 60\,k_{\mathrm{B}}T$.

The interaction between soluble and β-prone proteins is set by

$$V_{s\beta} = \begin{cases} -\varepsilon_{s\beta} & d \leq 1.3\,\sigma \\ 0 & d > 1.3\,\sigma \end{cases} \tag{3}$$

where d is the shortest distance between the attractive tip of the soluble protein and the side patch of the β-prone protein and $\varepsilon_{s\beta} = \varepsilon_{ss} + 1k_{\mathrm{B}}T$.

The coarse-grained implicit solvent model used here for the lipid membrane is defined in Ref. [19]. The membrane consists of three-bead lipids, which self-assemble into a stable bilayer.

The binding of the soluble protein to the membrane lipids is controlled by the interaction potential

$$V_{\mathrm{sm}} = \begin{cases} \infty & r \leq \sigma \\ -\varepsilon_{\mathrm{sm}}\left(\dfrac{\sigma}{r}\right)^6 & \sigma < r \leq 1.3\,\sigma \\ 0 & r > 1.3\,\sigma \end{cases} \tag{4}$$

where $\varepsilon_{\mathrm{sm}}$ is scaled by 1, 1/2, or 1/4 if the interacting lipid bead is either the head bead, the first or the second tail bead.

The second lipophilic side patch on the β-prone protein also has a length of 0.7ℓ and an opening angle of 180° and is oriented opposite to the $V_{\beta\beta}$-patch. It interacts only with the hydrophobic tail beads of the lipids via

$$V_{\beta\mathrm{m}} = \begin{cases} \infty & d \leq \sigma \\ -\varepsilon_{\beta\mathrm{m}}\cos^2\left[\dfrac{\pi}{2w_{c,\beta}}(r-\sigma)\right] & \sigma < d \leq \sigma + w_{c,\beta} \\ 0 & d > \sigma + w_{c,\beta} \end{cases} \tag{5}$$

where d denotes the minimal distance between the attractive patch and the corresponding lipid bead. The range of $V_{\beta m}$ between the proteins and the lipid is set to $w_{c,\beta} = \sigma$. The interaction strength $\varepsilon_{\beta\mathrm{m}}$ is set to 0 or $10\,k_{\mathrm{B}}T$, depending on the specific case under consideration.

Lipid beads interact repulsively via a Weeks-Chandler-Anderson potential given by

$$V_{l,r} = \begin{cases} 4\varepsilon\left[\left(\dfrac{b}{r}\right)^{12} - \left(\dfrac{b}{r}\right)^6 + \dfrac{1}{4}\right] & r \leq r_c \\ 0 & r > r_c \end{cases} \tag{6}$$

where $r_c = 2^{1/6}b$, $b_{\mathrm{head,head}} = b_{\mathrm{head,tail}} = 0.95\sigma$, and $b_{\mathrm{tail,tail}} = \sigma$. Beads of a three-bead lipid molecule are connected by two finitely extensible nonlinear elastic (FENE) bonds, described by

$$V_{\mathrm{l,bond}} = -\frac{k_{\mathrm{bond}}}{2}r_\infty^2\log\left[1 - \left(\frac{r}{r_\infty}\right)^2\right] \tag{7}$$

where $k_{\mathrm{bond}} = 30\,\varepsilon/\sigma^2$ and $r_\infty = 1.5\sigma$. Additionally, the head and second tail bead interact via the bending potential

$$V_{\mathrm{bend}} = \frac{k_{\mathrm{bend}}}{2}\,(r - 4\sigma)^2 \tag{8}$$

where $k_{\mathrm{bend}} = 10\,\varepsilon/\sigma^2$. The hydrophobic interactions between the lipid tails are account for by setting the attractive interaction between the two tail beads to

$$V_{l,a} = \begin{cases} -\varepsilon & r < r_c \\ -\varepsilon\cos^2\left[\dfrac{\pi}{2w_c}(r - r_c)\right] & r_c \leq r \leq r_c + w_c \\ 0 & r > r_c + w_c \end{cases} \tag{9}$$

with the ε and w_c being the depth and the range of the attractive potential, respectively. In this work, we set $w_c = 1.42\sigma$ and vary ε to prepare the lipid membrane in different phase state across the gel and fluid regime. In particular, we vary $k_{\mathrm{B}}T/\varepsilon$ between 0.775 (gel phase) and 1.135 (fluid). Note that the gel-fluid phase boundary is approximately located at $k_{\mathrm{B}}T/\varepsilon = 0.81$.

Monte-Carlo scheme The dynamics of the membrane-protein system is simulated by a Monte-Carlo scheme, which includes translational and rotational moves of individual particles. Additionally, the conversion between the soluble and β-prone conformation of the protein is also facilitated by a Metropolis criterion. This nucleated conformational change is accepted with probability $p = \min\{1, \mathrm{e}^{-\Delta E/k_\mathrm{B}T}\}$, where ΔE denotes the energy difference between the s and β-prone state. Switches between the two possible states are attempted with a probability of 0.01 per time step. These conformational changes between the s and the β state are penalised by the energy barrier $\Delta F_{s\to\beta} = 10\,k_\mathrm{B}T$. To suppress homogeneous nucleation in solution and speed up simulations, it is additionally required that a protein is lipid-bound to successfully switch states.

The simulations were carried out in a cubic simulation box with periodic boundaries in the x and y directions. The height of the box is kept constant at $L_z = 50\sigma$. The lengths L_x and L_y are allowed to fluctuate to keep the surface tension of the membrane constant at zero. Soluble proteins are equilibrated according to a grand-canonical ensemble with a fixed chemical potential keeping the concentration of soluble proteins constant in solution. Note that β-prone proteins follow the canonical ensemble. The membrane consists of 30×30 lipids in each leaf, amounting to 1800 three-bead lipids in total.

In a typical simulation run, proteins initially adsorb to the membrane while being maintained in the soluble conformation. After the equilibrium surface coverage is reached, the proteins are allowed to switch between the soluble and the β-sheet-prone state.

REFERENCES

* a.saric@ucl.ac.uk

[1] C. M. Dobson, Cold Spring Harbor Perspectives in Biology **9**, a023648 (2017).

[2] T. P. Knowles and R. Mezzenga, Advanced materials (Deerfield Beach, Fla.) **28**, 6546 (2016).

[3] S. Auer, A. Trovato, and M. Vendruscolo, PLoS Computational Biology **5**, e1000458 (2009).

[4] C. Cabaleiro-Lago, O. Szczepankiewicz, and S. Linse, Langmuir **28**, 1852 (2012).

[5] T. John, A. Gladytz, C. Kubeil, L. L. Martin, H. J. Risselada, and B. Abel, Nanoscale **10**, 20894 (2018).

[6] A. Morriss-Andrews and J.-E. Shea, The Journal of Chemical Physics **136**, 065103 (2012).

[7] R. Vácha, S. Linse, and M. Lund, Journal of the American Chemical Society **136**, 11776 (2014).

[8] M. Törnquist, T. C. T. Michaels, K. Sanagavarapu, X. Yang, G. Meisl, S. I. A. Cohen, T. P. J. Knowles, and S. Linse, Chemical Communications **54**, 8667 (2018).

[9] A. Šaric, A. K. Buell, G. Meisl, T. C. Michaels, C. M. Dobson, S. Linse, T. P. Knowles, and D. Frenkel, Nature Physics **12**, 874 (2016).

[10] P. K. Auluck, G. Caraveo, and S. Lindquist, Annual Review of Cell and Developmental Biology **26**, 211 (2010).

[11] G. Fusco, A. De Simone, P. Arosio, M. Vendruscolo, G. Veglia, and C. M. Dobson, Scientific Reports **6**, 1 (2016).

[12] A. Khondker, R. J. Alsop, and M. C. Rheinstädter, Membranes **7** (2017), 10.3390/membranes7030049.

[13] K. A. Burke, E. A. Yates, and J. Legleiter, Frontiers in Neurology **4**, 1 (2013).

[14] C. Galvagnion, A. K. Buell, G. Meisl, T. C. Michaels, M. Vendruscolo, T. P. Knowles, and C. M. Dobson, Nature Chemical Biology **11**, 229 (2015).

[15] C. Galvagnion, J. W. P. Brown, M. M. Ouberai, P. Flagmeier, M. Vendruscolo, A. K. Buell, E. Sparr, and C. M. Dobson, Proceedings of the National Academy of Sciences **113**, 7065 (2016).

[16] J. Habchi, S. Chia, C. Galvagnion, T. C. Michaels, M. M. Bellaiche, F. S. Ruggeri, M. Sanguanini, I. Idini, J. R. Kumita, E. Sparr, S. Linse, C. M. Dobson, T. P. Knowles, and M. Vendruscolo, Nature Chemistry **10**, 673 (2018).

[17] M. Yang, K. Wang, J. Lin, L. Wang, F. Wei, J. Zhu, W. Zheng, and L. Shen, Langmuir **34**, 8408 (2018).

[18] M. Bokvist, F. Lindström, A. Watts, and G. Gröbner, Journal of Molecular Biology **335**, 1039 (2004).

[19] I. R. Cooke and M. Deserno, Journal of Chemical Physics **123** (2005), 10.1063/1.2135785, arXiv:0509218 [cond-mat].

[20] A. Šarić, Y. C. Chebaro, T. P. J. Knowles, and D. Frenkel, Proceedings of the National Academy of Sciences **111**, 17869 (2014), arXiv:1412.0897.

[21] A. Šarić, T. C. T. Michaels, A. Zaccone, T. P. J. Knowles, and D. Frenkel, **211926** (2016), 10.1063/1.4965040, arXiv:1610.02320.

[22] G. Fusco, A. De Simone, T. Gopinath, V. Vostrikov, M. Vendruscolo, C. M. Dobson, and G. Veglia, Nature Communications **5**, 1 (2014).

[23] J. A. Hebda and A. D. Miranker, Annual Review of Biophysics **38**, 125 (2009).

[24] E. Terzi, G. Hölzemann, and J. Seelig, Journal of Molecular Biology **252**, 633 (1995).

[25] K. Matsuzaki, Biochimica et Biophysica Acta - Biomembranes **1768**, 1935 (2007).

[26] F. Hane, E. Drolle, R. Gaikwad, E. Faught, and Z. Leonenko, Journal of Alzheimer's Disease **26**, 485 (2011).

[27] H. Chaudhary, V. Subramaniam, and M. M. Claessens, ChemPhysChem **18**, 1620 (2017).

[28] G. Fusco, S. W. Chen, P. T. F. Williamson, R. Cascella, M. Perni, J. A. Jarvis, C. Cecchi, M. Vendruscolo, F. Chiti, N. Cremades, L. Ying, C. M. Dobson, and A. D. Simone, Science **1440**, 1 (2017).